Balance Control of a Simulated Inverted Pendulum on a Circular Base

Lukasz Wiklendt and Stephan Chalup
School of Electrical Engineering and Computer Science
The University of Newcastle
Callaghan, NSW 2308
lukasz.wiklendt@studentmail.newcastle.edu.au, stephan.chalup@newcastle.edu.au

Abstract

Balance control of a simulated inverted pendulum attached to a circular base is presented. This type of platform is analogous to a biped robot with circular soled feet in single support phase. Circular feet have been shown to be more energy efficient than flat feet during walking, and in this paper we present another advantage, where circular feet do not suffer from ground separation when applying a large torque at the ankle.

1 Introduction

The motivation for this type of platform is to investigate the potential for circular soles on robotic biped feet, hereafter called circular feet. We use the word "base" and "foot" interchangeably, depending on whether the focus is on the pendulum model or its application to a biped respectively. Although circular feet result in a point-contact with the ground, the practical difference between traditional point-contact feet (or single-point feet) is that for circular feet this point is available for control via the ankle joint. Throughout this paper we will assume that the foot cannot slide along the ground due to friction.

Using flat feet with no actuation at the ankle is analogous to point-contact feet, where the foot itself is considered a part of the ground, and the ankle represents the ground contact point. Attempting to apply torque to the ankle to introduce a degree of actuation requires the torque to be bounded so that one edge of the foot does not detach from the ground. If an edge detaches from the ground this effectively eliminates the actuation at the ground contact point. The range of this bound can be calculated using the Foot-Rotation Indicator (FRI) [Goswami, 1999], [Popovic *et al.*, 2005]. If the FRI moves outside the support area of the foot, then the opposite side of the foot will detach from the ground, effectively resulting in a single-point foot and loss of a degree of actuation. This is illustrated in Figure 1, showing point **A** detaching from the ground.

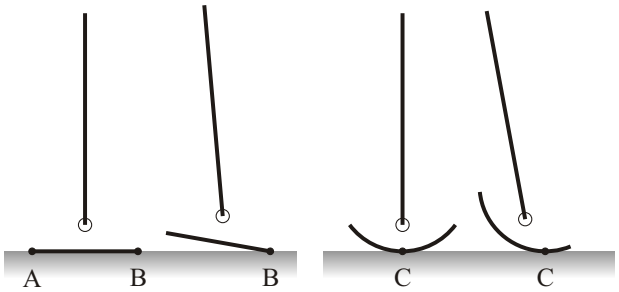

Figure 1: Left: effect of applying a torque at the ankle outside of the bounds which keep the FRI within the area of support for a flat foot. Ground contact point **A** detaches from the ground. Right: a circular foot does not suffer from this problem.

Using a circular foot there is no such restriction on the ankle torque. There is however a restriction on the angle the foot can subtend with the ground. If this angle is too large then the contact with the ground occurs at the edge of the foot, effectively creating a single-point foot. Circular feet also have advantages in passive dynamic walking [Asano and Luo, 2007], [Wisse *et al.*, 2005], [McGeer, 1990], and actuated walking with the ankle fused [Hase *et al.*, 2009], [Kinugasa *et al.*, 2009], [Morimoto *et al.*, 2004]. Examples of bipeds with round feet and actuated ankles for walking can be found in [Yeon *et al.*, 2006] and [Hosoda *et al.*, 2005]. If the ankle is located at the centre of the circle from which the arc base is derived, then the model resembles that of a planar robot on a spherical or wheeled base such as [Lauwers *et al.*, 2006] and [Kalra *et al.*, 2007]. Existing literature has focused on the locomotion aspects of bipeds with circular feet. In comparison, the contribution of this paper is a control mechanism to balance with circular feet when not in locomotion.

Flat feet have an advantage over circular feet when the biped is standing still. Static stability inherent in

flat feet allows a biped to remain balanced without any sensing and actuation, beyond keeping the ankle joint from rotating. This paper focuses on a control method useful in allowing a biped with curved feet to remain stable while standing. The method implemented is Linear Quadratic Control (LQR) [Anderson and Moore, 1971], which is the most popular method of control for linear time-invariant systems due to its robustness.

In the next section we show how the torque bound with a flat base motivated the investigation into a circular base. Section 3 describes the dynamic model of an inverted pendulum on a circular base, with a discussion on various radii of the base and their effects on the ankle locus. Section 4 contains the linearised equations of motion, results of a simulation under LQR balance control, and a region of successful balance control for various initial states. Section 5 briefly extends the study to an inverted double pendulum, showing the results of balance during a simulation similar to that conducted for an inverted single pendulum. Section 6 contains the conclusion.

2 Motivation

We investigate a planar inverted pendulum, modelling the pendulum as a rod and the base as a circle arc. A morphological comparison between a pendulum on a flat base and one on a circular base is illustrated in Figure 2. First, a description of the Foot-Rotation Indicator and how it applies to an inverted pendulum on a flat base is given. From [Goswami, 1999] the FRI "is the point on the foot/ground-contact surface where the net ground-reaction force would have to act to keep the foot stationary. To ensure no foot rotation, the FRI point must remain within the convex hull of the foot-support area." For a planar robot, the FRI point is calculated as

$$\begin{aligned} \mathrm{FRI}_x &= \frac{m_1 C_{1x} g - \sum_{i=2}^{N} I_i \ddot{\theta}_i}{m_1 g + \sum_{i=2}^{N} m_i \left(\ddot{C}_{iy} + g\right)} \\ &+ \frac{\sum_{i=2}^{N} m_i \left\{ C_{ix} \left(\ddot{C}_{iy} + g\right) - C_{iy} \ddot{C}_{ix} \right\}}{m_1 g + \sum_{i=2}^{N} m_i \left(\ddot{C}_{iy} + g\right)} \end{aligned} \quad (1)$$

where g is the acceleration due to gravity, and for link i; m_i is the mass, C_{ix} is the centre of mass in the x (horizontal) direction, C_{iy} is the centre of mass in the y (vertical) direction, I_i is the moment of inertia about the centre of mass, $\ddot{\theta}_i$ is the angular acceleration about link i's centre of mass. Link 1 represents the foot.

In the case of a planar inverted pendulum on a flat base in its initial state, that is, when the base is stationary and both ends are touching the ground, and the pendulum is stationary and completely upright, the FRI point is given by

$$\mathrm{FRI}_x^{init} = -\frac{(I_b + l(h+l)m_b)\,\ddot{\theta}_b}{g(m_f + m_b)} \quad (2)$$

where I_b is the moment of inertia of the pendulum about its centre of mass, l is half the length of the pendulum rod (and the distance of the centre of mass from each end), h is the height of the revolute joint from the base, g is the acceleration due to gravity, m_f and m_b are the masses of the base (foot) and the pendulum (body) respectively, $\ddot{\theta}_b$ is the angular acceleration of the pendulum about its centre of mass, and the centre of the base is at the origin.

Given w is the width of the foot then, in the initial state, one side of the foot will detach from the ground if

$$\left|\mathrm{FRI}_x^{init}\right| > \frac{w}{2} \quad (3)$$

converting the inverted pendulum on a flat base into an underactuated inverted serial double pendulum. See Figure 1 for an illustration of this effect. The bound on the maximum angular acceleration for states other than the initial can be calculated by substituting in (1).

This bound on the angular acceleration of the pendulum, and hence the torque about ankle, is the limit at which flat feet are no longer useful for flat support. Circular feet have no bound on the torque, as long as the foot radius r is larger than or equal to the height of the ankle ($r \geq h$) so that the robot does not become airborne by lifting its foot from the ground.

Irrespective of the torque applied at the ankle, even the smallest rotation of a flat foot results in one end of the foot detaching from the ground. If no rotation is desired then the FRI point must remain strictly within the area of support. In comparison, a circular foot is always in rotation when the FRI point doesn't exactly coincide with the ground contact point. However, rotation of a circular foot does not result in the dynamical model change to an inverted double pendulum, as long as the rotation doesn't move the ground contact point to the edge of the foot. Thus, in order to maintain dynamics of each model, a flat base is limited to 0 rotation and a circular base is limited to a maximum rotation of α, where α is half the central angle of the arc the base subtends.

3 Model

In this section the equations of motion of an inverted pendulum on a circular base are presented. The variables in the following equations are shown in Figure 3 for reference. The generalised coordinates of the system are the column vector $\mathbf{q} = \begin{pmatrix} \varphi & \theta \end{pmatrix}^\top$. Lagrangian

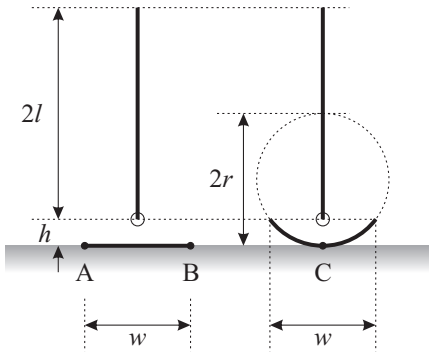

Figure 2: Flat base and circular base inverted pendulum models, where l is the distance from the ankle (shown as a small circle) to the centre of mass of the pendulum rod.

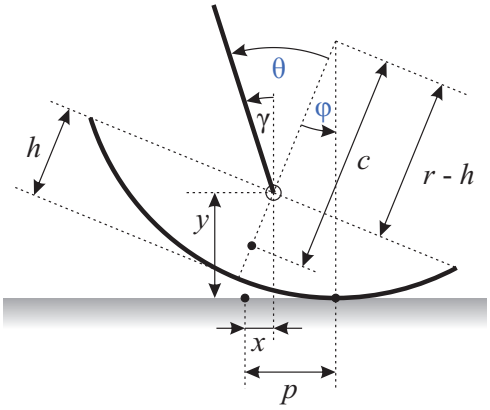

Figure 3: Parameters and state variables of an inverted pendulum on a circular base. Parameters and state variables are shown in black and blue respectively.

mechanics is used to solve for accelerations in these coordinates.

Some derived variables useful in simplifying the equations for kinetic and potential energy are

$$
\begin{aligned}
p &= \varphi r && (4)\\
\gamma &= \theta - \varphi && (5)\\
x &= p - (r-h)\sin(\varphi) && (6)\\
y &= r - (r-h)\cos(\varphi) && (7)\\
c &= \frac{r\sin(\alpha)}{\alpha} && (8)\\
C_{bx} &= x - l\sin(\gamma) && (9)\\
C_{by} &= y + l\cos(\gamma) && (10)\\
C_{fx} &= p - c\sin(\varphi) && (11)\\
C_{fy} &= r - c\cos(\varphi) && (12)
\end{aligned}
$$

where c is the distance from the centre of the circle to the centroid, and α is half the central angle of the arc base. From Figure 3 we can deduce that $\alpha = \cos^{-1}((r-h)/r)$, although the central angle's condition on r and h is not necessary and can be adjusted to reduce or extend the maximum allowed foot rotation. The following two assumptions are maintained: the condition $\varphi \leq \alpha$ always holds, that is, the foot never rolls past its ends, and the foot is always in contact with the ground.

The kinetic energy of the system is

$$
\begin{aligned}
T_b &= \frac{1}{2}I_b\dot{\gamma}^2 + \frac{1}{2}m_b\left(\dot{C}_{bx}^2 + \dot{C}_{by}^2\right) && (13)\\
T_f &= \frac{1}{2}I_f\dot{\varphi}^2 + \frac{1}{2}m_f\left(\dot{C}_{fx}^2 + \dot{C}_{fy}^2\right) && (14)\\
T &= T_b + T_f && (15)
\end{aligned}
$$

where the moments of inertia are given by

$$
\begin{aligned}
I_b &= \frac{1}{12}m_b(2l)^2 && (16)\\
I_f &= m_f(r^2 - c^2) && (17)
\end{aligned}
$$

and the potential energy of the system is

$$
V = g\left(m_b C_{by} + m_f C_{fy}\right) \quad (18)
$$

Applying this to the Lagrange formula

$$
\begin{aligned}
\mathcal{L} &= T - V && (19)\\
\frac{d}{dt}\left(\frac{\delta\mathcal{L}}{\delta\dot{\mathbf{q}}}\right) - \frac{\delta\mathcal{L}}{\delta\mathbf{q}} &= \begin{pmatrix} 0 \\ \tau \end{pmatrix} && (20)
\end{aligned}
$$

for each generalised coordinate gives the following equations of motion[1]

$$
\mathbf{D}(\mathbf{q})\ddot{\mathbf{q}} + \mathbf{C}(\mathbf{q},\dot{\mathbf{q}}) + \mathbf{G}(\mathbf{q}) = \begin{pmatrix} 0 \\ \tau \end{pmatrix} \quad (21)
$$

where the elements of the matrices $\mathbf{D}$, $\mathbf{C}$, and $\mathbf{G}$ are

$$
\begin{aligned}
d_{11} &= I_b + I_f + h^2 m_b + l^2 m_b + c^2 m_f \\
&\quad +2\cos(\theta) l m_b (h-r) - 2h m_b r \\
&\quad +2\cos(\varphi) h m_b r + 2\cos(\gamma) l m_b r \\
&\quad -2\cos(\varphi) c m_f r + 2 m_b r^2 \\
&\quad -2\cos(\varphi) m_b r^2 + m_f r^2 \\
d_{12},\ d_{21} &= l m_b(\cos(\theta)(r-h) - \cos(\gamma) r - l) - I_b \\
d_{22} &= I_b + l^2 m_b \\
c_1 &= a r\dot{\varphi}^2 - 2b\dot{\varphi}\dot{\theta} + b\dot{\theta}^2 \\
c_2 &= l m_b (h-r)\sin(\theta)\dot{\varphi}^2 \\
g_1 &= ag \\
g_2 &= -g l m_b \sin(\gamma) \\
a &= l m_b \sin(\gamma) + (-h m_b + c m_f + m_b r)\sin(\varphi) \\
b &= l m_b (r(\sin(\gamma) - \sin(\theta)) + h\sin(\theta))
\end{aligned}
$$

where m_b represents the mass of the pendulum (body), and m_f represents the mass of the base (foot).

[1] derived with the Mathematica [Wolfram Research, Inc., 2008] computer algebra system.

3.1 Circular Base Radius

The choice of radius for the circular base affects the ankle locus. For passive dynamics walkers it is advised not to use a radius larger than the leg length, with suggestions of a third of the leg length [Kinugasa *et al.*, 2009]. Effects of various radii on the metabolic costs of walking were explored in [Adamczyk *et al.*, 2006]. In this section we mention how the difference in distance Δd between the ankle and the original centre of mass of the pendulum changes as the foot rolls over the ground, varying φ. The difference in distance is given by

$$\Delta d \quad = \quad l - \sqrt{x^2 + (y - (h + l))^2} \tag{22}$$

This allows one to choose an arc radius of the foot such that the rolling of the foot minimises the change in centre of mass of the pendulum due to the ankle pulling or pushing on the pendulum. Figure 4 shows Δd for a range of foot radii as φ changes. It can be thought of as the ankle locus as seen from the initial-state pendulum centre of mass. Equation (22) is chosen as the negative of an intuitive distance difference to better illustrate the locus of the ankle. In Figure 4 we can see that as the radius increases the locus approaches the cusp of a flat foot ankle locus.

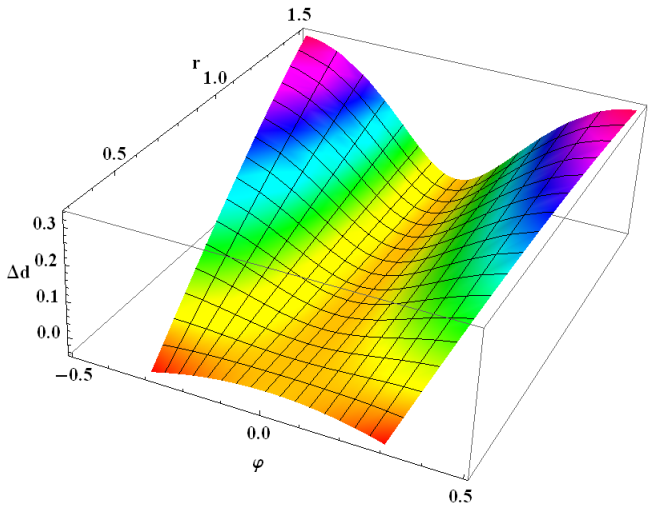

Figure 4: Difference in distance between the ankle at various φ and the pendulum centre of mass at $\varphi = 0$ for various r, where $l = 1$ and $h = 0.3$. Negative Δd represents a larger distance and positive a smaller distance.

4 LQR Balance Control

One disadvantage of circular feet is that the robot requires constant control to remain upright even when standing practically still. This section addresses this issue by presenting a balance controller for the robot, allowing a stationary upright state to be maintained in the presence of minor disturbances.

The continuous-time linear time-invariant system obtained by linearising the equations of motion (21) about $\begin{pmatrix} \varphi & \theta & \dot{\varphi} & \dot{\theta} \end{pmatrix}^\top = \mathbf{0}$ is given by

$$\dot{\mathbf{x}} \quad = \quad A\mathbf{x} + B\tau \tag{23}$$

where

$$A \quad = \quad \begin{pmatrix} 0 & 0 & 1 & 0 \\ 0 & 0 & 0 & 1 \\ a_{31} & a_{32} & 0 & 0 \\ a_{41} & a_{42} & 0 & 0 \end{pmatrix} \tag{24}$$

$$B \quad = \quad \begin{pmatrix} 0 \\ 0 \\ b_{31} \\ b_{41} \end{pmatrix} \tag{25}$$

$$\mathbf{x} \quad = \quad \begin{pmatrix} \varphi & \theta & \dot{\varphi} & \dot{\theta} \end{pmatrix}^\top \tag{26}$$

$$a_{31} \quad = \quad \frac{g\left(hI_b m_b - \left(I_b + l^2 m_b\right)\left(cm_f + m_b r\right)\right)}{d}$$

$$a_{32} \quad = \quad \frac{ghl^2 m_b^2}{d}$$

$$a_{41} \quad = \quad -\frac{g}{d}\left(cI_b m_f + hm_b(-I_b + clm_f + lm_b r)\right.$$
$$+ m_b\left(I_b r + l\left(I_{ft} + c^2 m_f + cm_f(l - 2r)\right.\right.$$
$$+ \left.\left. r(lm_b + m_f r)\right)\right)$$

$$a_{42} \quad = \quad \frac{glm_b(I_{ft} + h(h + l)m_b + m_f(c - r)^2)}{d}$$

$$b_{31} \quad = \quad \frac{I_b + l(h + l)m_b}{d}$$

$$b_{41} \quad = \quad \frac{I_b + I_{ft} + (h + l)^2 m_b + m_f(c - r)^2}{d}$$

$$d \quad = \quad l^2 m_b(I_{ft} + m_f(c - r)^2)$$
$$+ I_b(I_{ft} + h^2 m_b + m_f(c - r)^2)$$

The value of the gain K which minimises the quadratic cost function

$$J \quad = \quad \int_0^\infty \left(\mathbf{x}^\top Q\mathbf{x} + R\tau^2\right) dt \tag{27}$$

for the state-feedback control law

$$\tau \quad = \quad -K\mathbf{x} \tag{28}$$

can be found by solving the continuous-time algebraic Riccati equation for P

$$A^\top P + PA - PBR^{-1}B^\top P + Q = 0 \tag{29}$$

and setting

$$K \quad = \quad R^{-1}B^\top P \tag{30}$$

The Matlab [MathWorks, Inc., 2008] '`lqr`' function was used in solving equation (29), which at the time of use implemented [Arnold III and Laub, 1984].

4.1 Balance Simulation

An inverted pendulum was simulated using equation (21), by applying torque specified by equation (28). Figure 5 shows results of the first 1.2 seconds of simulation. Model parameters used are shown in Table 1, and the weight matrices for the cost function in equation (27) were set to $Q = \texttt{diag}(10, 1, 0.1, 0.1)$ and $R = 1$. The Q weight matrix was designed by hand to emphasise the cost of φ deviating from 0, in order to help prevent the base from rotating such that the ground contact point coincides with the edge of the base.

l	r	h	m_b	m_f	g
0.5	0.0625	0.025	1	0.1	9.81

Table 1: Parameters used for simulation.

The value of the gain feedback matrix for these parameters was calculated to be

$$K \approx \begin{pmatrix} -81.4 & 78.2 & 21.6 & 21.9 \end{pmatrix} \quad (31)$$

Although not visible from Figure 5, the torque started at a value of $\tau \approx 6.1$N, then rapidly decreased to it's local minimum at around 0.004 seconds, then the gradual increase and eventual decline is visible in the plot.

To measure the efficacy of the balancing controller where the pendulum is subject to disturbances from the the equilibrium point, the pendulum was initialised to various states and then simulated under LQR control with the same parameters as described above. An unsuccessful balance was defined as the foot rotating past its edge ($|\varphi| > \alpha$), or the pendulum subtending an angle greater than $\frac{\pi}{2}$ from the vertical ($|\gamma| > \frac{\pi}{2}$). Otherwise the balance was considered successful. Each simulation was run for 2 seconds, which was enough to determine whether the balance control would succeed, since for an unsuccessful balance the pendulum would either topple or the foot would rotate past its ends well before the 2 second simulation finished. The longest unsuccessful balance simulation lasted 0.434 seconds before the aforementioned failing criteria were satisfied. Figure 6 shows initial states leading to successful balances under control of the LQR balancing controller.

5 Double Pendulum

The single-rod pendulum presented so far has been useful in illustrating the differences between a circular foot and a flat foot. Humanoid robots usually have hip joints, which allow for a greater range of initial states from which the robot is able to balance. In this section a simulation of a double pendulum on a circular base is presented, where the joint between the two pendulum rods represents the hip (see Figure 7).

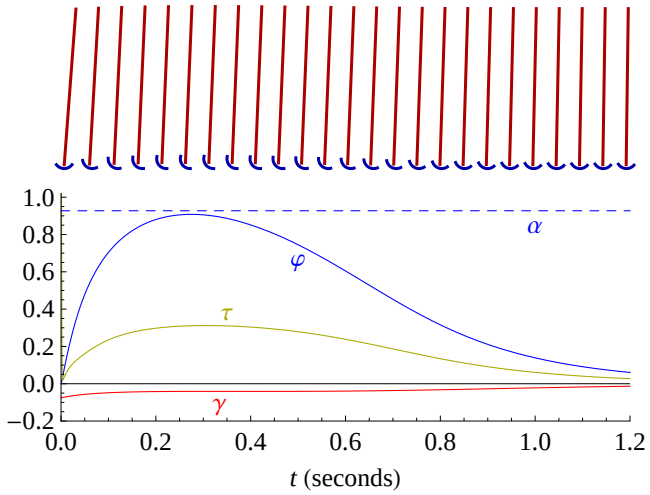

Figure 5: Simulation of balancing an inverted pendulum on a circular base for 1.2 seconds (see Video 1). Initial angle of the pendulum was $\theta = -0.075$ rad, and all other state values were initialised to 0. *Top*: Frames from the video in chronological order. *Bottom*: State and torque vs time, vertically aligned with the top image. The coloured solid curves show the progression of the corresponding state and input values. The blue dashed horizontal line represents α, that is, when the ground contact point would coincide with the edge of the foot.

The equations of motion are more complex than those for the single pendulum. To keep clutter to a minimum the same symbols will be used as for the single pendulum, but redefined for this section. The generalised coordinates are $\mathbf{q} = \begin{pmatrix} \varphi & \theta_1 & \theta_2 \end{pmatrix}^\top$. The equations of motion are given by

$$\mathbf{D}(\mathbf{q})\ddot{\mathbf{q}} + \mathbf{C}(\mathbf{q}, \dot{\mathbf{q}}) + \mathbf{G}(\mathbf{q}) = \begin{pmatrix} 0 \\ \tau_1 \\ \tau_2 \end{pmatrix} \quad (32)$$

where the elements of the matrices $\mathbf{D}$, $\mathbf{C}$, and $\mathbf{G}$ are too verbose to be presented here and can be found in the Appendix.

5.1 LQR Balance Control and Simulation

Calculating the gain feedback matrix for the double pendulum was performed in the same way as for the single

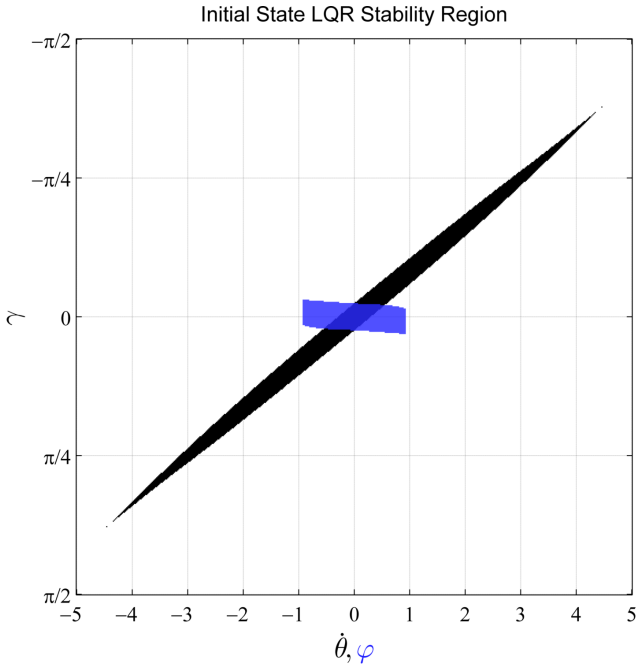

Figure 6: The black region indicates a successful LQR balance for various initial γ and $\dot{\theta}$, where φ and $\dot{\varphi}$ were initialised to 0. The translucent blue region indicates a successful LQR balance for various initial γ and φ, where $\dot{\theta}$ and $\dot{\varphi}$ were initialised to 0. Note that $|\varphi| \leq \alpha$, where $\alpha \approx 0.93$ represents a foot rotation such that the ground contact point coincides with the edge of the foot.

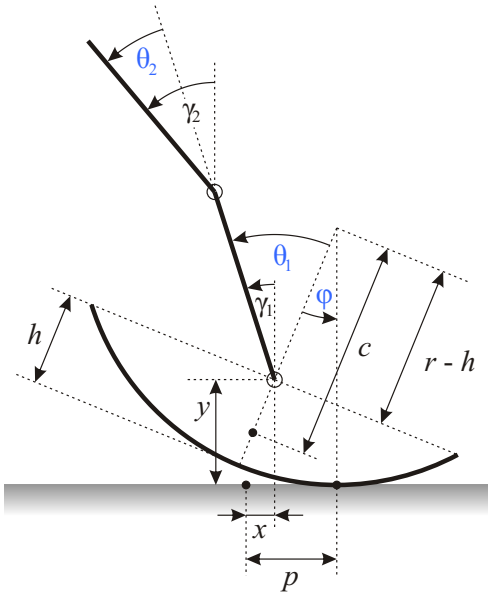

Figure 7: Parameters and state variables of an inverted double pendulum on a circular base. Parameters and state variables are shown in black and blue respectively.

pendulum. The cost function is given by

$$J = \int_0^\infty \left(\mathbf{x}^\top Q\mathbf{x} + \mathbf{u}^\top R\mathbf{u}\right) dt \tag{33}$$

for the state and input vectors

$$\mathbf{x} = \begin{pmatrix} \varphi & \theta_1 & \theta_2 & \dot{\varphi} & \dot{\theta}_1 & \dot{\theta}_2 \end{pmatrix}^\top \tag{34}$$

$$\mathbf{u} = \begin{pmatrix} \tau_1 & \tau_2 \end{pmatrix}^\top \tag{35}$$

where the cost matrices were set to

$$Q = \mathtt{diag}(10, 1, 1, 0.1, 0.1, 0.1) \tag{36}$$

$$R = \mathtt{diag}(1, 1) \tag{37}$$

For parameters given in Table 2, the value of the LQR gain feedback matrix was calculated to be

$$K \approx \begin{pmatrix} -65 & 69 & 19 & -18 & 18 & 6 \\ 34 & -34 & -6 & 9 & -9 & -2 \end{pmatrix} \tag{38}$$

The first 1.5 seconds of simulation are shown in Figure 8. Not visible in the plot, the torques started at $\tau_1 \approx 6.2$N and $\tau_2 \approx -3$N. Similar to the single pendulum simulation, the τ_1 declined rapidly to about 0.004 seconds into the simulation, then gradually rose and eventually decline as can be seen in the plot. The torque τ_2 increased monotonically for the period outside the plot's range.

l_1, l_2	r	h	m_1, m_2	m_f	g
0.25	0.0625	0.025	0.5	0.1	9.81

Table 2: Double pendulum parameters used for simulation, where l_1, m_1, and l_2, m_2 represent half the lengths and the masses of the first and second pendulum rods respectively, counting from the ankle.

6 Conclusion

A benefit of circular feet over flat feet is that the limit of available control shifts from being both state and torque bound with a flat foot to only state bound with a circular foot. In addition to this and the benefits already mentioned in literature, a circular foot with an actuated ankle allows a biped to maintain partial control of the ground-contact point, similar to the complete control offered by robots on wheels. However, a circular footed pendulum is always unstable, and requires constant balance control to remain standing.

If the benefits mentioned in this paper, and the benefits to energy efficiency and smooth rolling motion mentioned in other literature out-weigh this restriction then circular or rounded feet should be considered as an alternative to flat feet.

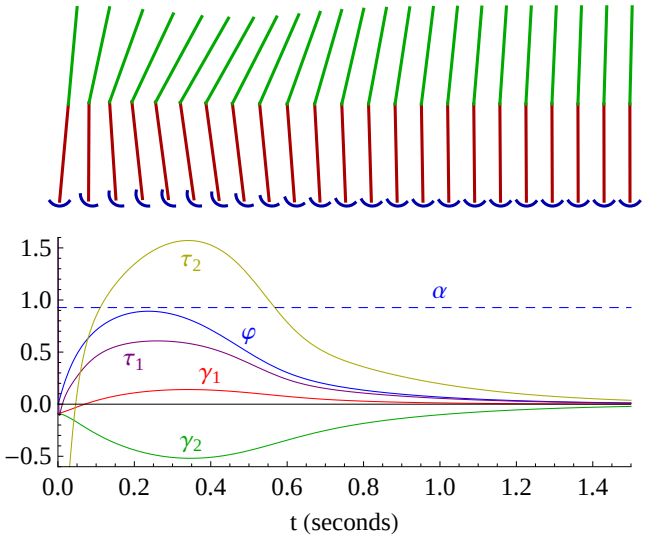

Figure 8: Simulation of balancing an inverted double pendulum on a circular base for 1.5 seconds (see Video 2). Initial angle of the pendulum was $\theta_1 = -0.09$ rad, and all other state values were initialised to 0. *Top*: Frames from the video in chronological order. *Bottom*: State and torque vs time, vertically aligned with the top image. The coloured solid curves show the progression of the corresponding state and input values. The blue dashed horizontal line represents α, that is, when the ground contact point would coincide with the edge of the foot.

Appendix: Double Pendulum Dynamics

The equations of motion[2] for an inverted double pendulum on a circular base are given by

$$\mathbf{D}(\mathbf{q})\ddot{\mathbf{q}} + \mathbf{C}(\mathbf{q},\dot{\mathbf{q}}) + \mathbf{G}(\mathbf{q}) = \begin{pmatrix} 0 \\ \tau_1 \\ \tau_2 \end{pmatrix}$$

where the elements of the above matrices are given by

$$\begin{aligned}
d_{11} &= I_1 + I_2 + I_f + h^2 m_1 + l_1^2 m_1 + h^2 m_2 \\
&+ 4l_1^2 m_2 + l_2^2 m_2 + c^2 m_f - 2h(m_1+m_2)r \\
&+ (2(m_1+m_2)+m_f)r^2 \\
&+ 2l_1(m_1+2m_2)(h-r)\cos(\theta_1) \\
&+ 4l_1 l_2 m_2 \cos(\theta_2) \\
&+ 2(l_2 m_2 (h-r)\cos(\theta_1+\theta_2) \\
&+ r(l_1(m_1+2m_2)\cos(\gamma_1) \\
&+ l_2 m_2 \cos(\gamma_2) \\
&+ (-cm_f + (m_1+m_2)(h-r))\cos(\varphi))) \qquad (39)
\end{aligned}$$

$$\begin{aligned}
d_{12}, d_{21} &= -I_1 - I_2 - l_1^2 m_1 - 4l_1^2 m_2 - l_2^2 m_2 \\
&- l_1(m_1+2m_2)(h-r)\cos(\theta_1) \\
&- 4l_1 l_2 m_2 \cos(\theta_2) - h l_2 m_2 \cos(\theta_1+\theta_2) \\
&+ l_2 m_2 r \cos(\theta_1+\theta_2) \\
&- l_1 m_1 r \cos(\gamma_1) - 2l_1 m_2 r \cos(\gamma_1) \\
&- l_2 m_2 r \cos(\gamma_2) \\
d_{13}, d_{31} &= -I_{b_2} - l_2^2 m_2 \\
&- l_2 m_2 (2l_1 \cos(\theta_2) + (h-r)\cos(\theta_1+\theta_2) \\
&+ r\cos(\gamma_2)) \\
d_{22} &= I_1 + I_2 + l_2^2 m_2 + l_1^2(m_1+4m_2) \\
&+ 4l_1 l_2 m_2 \cos(\theta_2) \\
d_{23}, d_{32} &= I_2 + l_2^2 m_2 + 2l_1 l_2 m_2 \cos(\theta_2) \\
d_{33} &= I_2 + l_2^2 m_2
\end{aligned}$$

$$\begin{aligned}
c_1 &= ((h-r+r\cos(\varphi))(l_1(m_1+2m_2)\sin(\theta_1) \\
&+ l_2 m_2 \sin(\theta_1+\theta_2)) \\
&- r(l_1(m_1+2m_2)\cos(\theta_1) \\
&+ l_2 m_2 \cos(\theta_1+\theta_2))\sin(\varphi))\dot{\theta}_1^2 \\
&+ 2l_2 m_2 (2l_1 \sin(\theta_2) + (h-r)\sin(\theta_1+\theta_2) \\
&+ r\sin(\gamma_2))\dot{\theta}_1\dot{\theta}_2 + l_2 m_2 (2l_1 \sin(\theta_2) \\
&+ (h-r)\sin(\theta_1+\theta_2) + r\sin(\gamma_2))\dot{\theta}_2^2 \\
&+ (-2((h-r+r\cos(\varphi))(l_1(m_1+2m_2)\sin(\theta_1) \\
&+ l_2 m_2 \sin(\theta_1+\theta_2)) - r(l_1(m_1+2m_2)\cos(\theta_1) \\
&+ l_2 m_2 \cos(\theta_1+\theta_2))\sin(\varphi))\dot{\theta}_1 \\
&- 2l_2 m_2 (2l_1 \sin(\theta_2) + (h-r)\sin(\theta_1+\theta_2) \\
&+ r\sin(\gamma_2))\dot{\theta}_2)\dot{\varphi} + r(l_1(m_1+2m_2)\sin(\gamma_1) \\
&+ l_2 m_2 \sin(\gamma_2) \\
&+ (cm_f - (m_1+m_2)(h-r))\sin(\varphi))\dot{\varphi}^2 \\
c_2 &= -4l_1 l_2 m_2 \sin(\theta_2)\dot{\theta}_1\dot{\theta}_2 \\
&- 2l_1 l_2 m_2 \sin(\theta_2)\dot{\theta}_2^2 + 4l_1 l_2 m_2 \sin(\theta_2)\dot{\theta}_2\dot{\varphi} \\
&+ (h-r)(l_1(m_1+2m_2)\sin(\theta_1) \\
&+ l_2 m_2 \sin(\theta_1+\theta_2))\dot{\varphi}^2 \\
c_3 &= 2l_1 l_2 m_2 \sin(\theta_2)\dot{\theta}_1^2 - 4l_1 l_2 m_2 \sin(\theta_2)\dot{\theta}_1\dot{\varphi} \\
&+ l_2 m_2 (2l_1 \sin(\theta_2) + (h-r)\sin(\theta_1+\theta_2))\dot{\varphi}^2
\end{aligned}$$

$$\begin{aligned}
g_1 &= g(l_1(m_1+2m_2)\sin(\gamma_1) \\
&+ l_2 m_2 \sin(\theta_1+\theta_2-\varphi(t))) \\
&+ (cm_f - (m_1+m_2)(h-r))\sin(\varphi) \\
g_2 &= -g(l_1(m_1+2m_2)\sin(\gamma_1) + l_2 m_2 \sin(\gamma_2)) \\
g_3 &= -g l_2 m_2 \sin(\gamma_2)
\end{aligned}$$

[2] derived with the Mathematica [Wolfram Research, Inc., 2008] computer algebra system.

References

[Adamczyk *et al.*, 2006] P.G. Adamczyk, S.H. Collins, and A.D. Kuo. The advantages of a rolling foot in human walking. *Journal of Experimental Biology*, 209(20):3953–3963, 2006.

[Anderson and Moore, 1971] B.D.O. Anderson and J.B. Moore. *Linear Optimal Control*. Prentice Hall, 1971.

[Arnold III and Laub, 1984] W.F. Arnold III and A.J. Laub. Generalized eigenproblem algorithms and software for algebraic riccati equations. *Proceedings of the IEEE*, 72(12):1746–1754, 1984.

[Asano and Luo, 2007] F. Asano and Zhi-Wei Luo. The effect of semicircular feet on energy dissipation by heel-strike in dynamic biped locomotion. In *Robotics and Automation, 2007 IEEE International Conference on*, pages 3976–3981, April 2007.

[Goswami, 1999] A. Goswami. Postural stability of biped robots and the foot-rotation indicator (FRI) point. *The International Journal of Robotics Research*, 18(6):523–533, 1999.

[Hase *et al.*, 2009] Takamasa Hase, Qingjiu Huanga, and Xuedong Chen. Performance analysis of biped walking robot with circular feet using optimal trajectory planning method. In *Robotics and Biomimetics. Proceedings of the 2008 IEEE International Conference on*, February 2009.

[Hosoda *et al.*, 2005] K. Hosoda, T. Takuma, and M. Ishikawa. Design and control of a 3d biped robot actuated by antagonistic pairs of pneumatic muscles. *Proceedings of 3rd International Symposium on Adaptive Motion in Animals and Machines, CD–ROM, Sep*, 2005.

[Kalra *et al.*, 2007] S. Kalra, D. Patel, and K. Stol. Design and hybrid control of a two wheeled robotic platform. In *Proceedings 2007 Australasian Conference on Robotics and Automation*, 2007.

[Kinugasa *et al.*, 2009] T. Kinugasa, C. Chevallereau, and Y. Aoustin. Effect of circular arc feet on a control law for a biped. *Robotica*, 27(04):621–632, July 2009.

[Lauwers *et al.*, 2006] T.B. Lauwers, G.A. Kantor, and R.L. Hollis. A dynamically stable single-wheeled mobile robot with inverse mouse-ball drive. In *Proceedings of IEEE International Conference on Robotics and Automation*, pages 2884–2889, 2006.

[MathWorks, Inc., 2008] MathWorks, Inc. *MATLAB R2008a*. MathWorks, Inc., 7.6 edition, 2008.

[McGeer, 1990] T. McGeer. Passive dynamic walking. *The International Journal of Robotics Research*, 9(2):62–82, 1990.

[Morimoto *et al.*, 2004] J. Morimoto, J. Nakanishi, G. Endo, and G. Cheng. Acquisition of a biped walking pattern using a poincare map. In *Humanoid Robots, 2004 4th IEEE/RAS International Conference on*, volume 2, pages 912–924 Vol. 2, Nov. 2004.

[Popovic *et al.*, 2005] M.B. Popovic, A. Goswami, and H. Herr. Ground reference points in legged locomotion: Definitions, biological trajectories and control implications. *The International Journal of Robotics Research*, 24(12):1013–1032, 2005.

[Wisse *et al.*, 2005] M. Wisse, A.L. Schwab, R.Q. van der Linde, and F.C.T. van der Helm. How to keep from falling forward: elementary swing leg action for passive dynamic walkers. *IEEE Transactions on Robotics*, 21(3):393–401, 2005.

[Wolfram Research, Inc., 2008] Wolfram Research, Inc. *Mathematica*. Wolfram Research, Inc. Champaign, Illinois, 7.0 edition, 2008.

[Yeon *et al.*, 2006] J.S. Yeon, O. Kwon, and J.H. Park. Trajectory generation and dynamic control of planar biped robots with curved soles. *Journal of Mechanical Science and Technology*, 20(5):602–611, 2006.